Extended phonon-scattering mechanism as an explanation for low mobility in highly concentrated electron layers at silicon interfaces

H. Benisty and J.-N. Chazalviel
Laboratoire de Physique de la Matière Condensée, Ecole Polytechnique, 91128 Palaiseau CEDEX, France
(Received 14 December 1989)

Mobility data for electrons in very-high-density accumulation layers at the Si(111)/polymer-electrolyte interface are presented which identify phonons as the major scattering source even in this density range. Next we present a revised treatment of usual acoustic-phonon and intervalley-phonon scattering mechanisms including the case of a degenerate Si(111) two-dimensional electron gas. However, this approach overestimates the experimental ~ 100 cm^2/V s mobilities by a factor of 5–10. Hence, a new extended scattering mechanism by acoustic phonons is proposed which accounts for these low mobilities as well as for those observed in concentrated accumulation and inversion layers at the Si/SiO_2 interface around room temperature. This is done by using the $\mathbf{k}\cdot\mathbf{p}$ expansion of the phonon-scattering matrix element one order higher than the usual deformation-potential mechanism in order to establish a simplified expression which is further adapted to the two-dimensional case. A simple interpretation is proposed, consisting of a deformation-induced displacement of the position of valley minima in reciprocal space. Finally, the order of magnitude of this new mechanism is explained by considering the vicinity of the conduction-band minima relative to the Brillouin-zone edges.

I. INTRODUCTION

Electron accumulation (inversion) layers at the surface of *n*-type (*p*-type) silicon, a well-known two-dimensional electron gas (2D EG),[1,2] exhibit low mobilities (less than 400 cm^2/V s) at high concentrations ($N_s > 5\times10^{12}e^-$/cm^2) around room temperature (100–500 K):[3] In this range, phonon scattering is expected to be dominant, as confirmed by the temperature dependence of the mobility. In such systems, however, "the theory of phonon scattering is. . . at an unsatisfactory stage," as Ando *et al.* remarked in their 1982 review article,[1] because of the largely overestimated mobility values obtained by adapting the usual deformation-potential theory to 2D EG. Attempts by Ezawa *et al.* in the early 1970s to take into account the exact phonon interface modes yielded limited results.[4] It was also proposed that "surface deformation potentials" should be noticeably greater than their bulk counterparts.[5,6] Such approaches were not confirmed, and owing to the limited work carried out on this problem since then, the 1982 statement of Ando *et al.* remains essentially valid.

The recent demonstration that (*n*-type Si)/indifferent-electrolyte interfaces can circumvent the density limitation of the Si/insulator interfaces classically used for creating 2D EG's has opened the way to new investigations.[7–9] It is instructive to compare these two systems: in both cases the interface is polarized in order to accumulate electrons on the silicon side. In standard metal-insulator-semiconductor (MIS) structures,[2] the corresponding positive countercharge lies in the metallic gate and a relatively large electric field is present across the insulator (e.g., oxide) layer. On the other hand, in a Si/electrolyte interface, the countercharge can be seen as an accumulation of cations, which are able to screen the electronic charge within only atomic distances of the silicon surface.[10] This is the narrow double layer[11] (the so-called Helmholtz layer) where the electric field is very large but over one or two nanometers at most.

For this reason, the polarization is limited by very different processes in these two systems: in MIS structures, breakdown[2] in the insulator prevents densities larger than $1\sim2\times10^{13}e^-$/cm^2. It arises from carrier acceleration inside the relatively thick insulator layer. On the other hand, Faradaic currents are the limiting process at the Si/electrolyte interface:[7] beyond a given polarization, electrons can be transferred to the electrolyte, inducing an electrochemical reaction. This limitation is far more intrinsic than breakdown: it does not rely on insulator defects but on the availability of "empty electronic levels" in the electrolyte; Faradaic currents arise only when the Fermi level of silicon is aligned to these electronic levels due to the polarization.[12] The relevant electrochemical concept for this naive image is the "domain of stability" of the electrolyte. To accumulate electrons, we are interested in the "cathodic" limit of this domain, i.e., a negative electrode potential for the electrochemists who usually refer to the potential of the solution[13]—as in this paper—whereas the similar situation for a usual MIS structure corresponds to a positive gate (metal) potential. The cathodic limit of the domain of stability of the electrolyte finally reflects the energetical cost for an electron to be transferred from silicon to the electrolyte. It is thus a key factor to maximize accumulation at the Si/electrolyte interface. Fortunately, for "indifferent" electrolytes such as acetonitrile+0.1*M* alkaline salt, the

onset of Faradaic currents takes place only at very strong (cathodic) polarizations (−2.5 V): at such strong polarizations, surface densities N_s of almost $10^{14}e^-/cm^2$ have been reached at [n-type Si(111)]/electrolyte interfaces at room temperature.[7] This is almost a 1-order-of-magnitude increase with respect to MIS structures.

At such high densities, these "giant" accumulation layers offer the unique opportunity of a quasidegenerate 2D EG at room temperature. Conductivity measurements indicate that, at these large concentrations, the electronic mobility decreases to ~50 $cm^2/V\,s$ at $8\times10^{13}e^-/cm^2$ while its dependence as a function of density lies between $N_s^{-1/6}$ and $N_s^{-1/2}$, a behavior compatible with a phonon-scattering mechanism.[7]

It was further shown that very-high-density accumulation layers up to $4.5\times10^{13}e^-/cm^2$ can be created at an all-solid interface using indifferent polymer electrolytes.[9,14] These electrolytes consist of a very-high-molecular-weight poly(ethyleneoxide) $[CH_2—CH_2—O—)]_n$ "solvent" (PEO) solvating a suitable salt such as $KClO_4$ or $CsCF_3SO_3$. The whole polymer electrolyte will be abbreviated as PEO. We report here on the results obtained with these Si(111)/PEO interfaces in the 300–400 K range. Furthermore, the results obtained from an [n-type Si(111)]/methanol-electrolyte interface in the 200–300 K range will also be used.[14]

Section II is devoted to the experimental results. The mobility limited by acoustic-phonon and intervalley-phonon scattering in Si(111) 2D EG is calculated in Sec. III. Taking advantage of the equivalence between the six valleys for the Si(111) surface, we present a treatment in the one-subband approximation which corrects previous ones, clarifying some misconceptions which appeared in the literature regarding the intervalley-phonon choice (Sec. III A) and the treatment of degeneracy (Sec. III B). Using deformation potentials of bulk silicon, this theory is shown to yield mobility values overestimated by a factor of 5–10.

This discrepancy motivates the attempt of Sec. IV to formulate a new mechanism, specific to highly concentrated electron accumulation layers. We suggest that at these high densities the whole change of the band structure induced by the acoustic-phonon perturbation must be taken into account. An intuitive approach is presented in Sec. IV A: the next step beyond the uniform shift approximation amounts to considering a phonon-induced displacement of the position of conduction-band minima in reciprocal space. The resulting expression is justified in Sec. IV B, using the 30-year-old $\mathbf{k}\cdot\mathbf{p}$ expansion of the electron-phonon interaction in nonpolar semiconductors from Harrison;[15] a simplified three-dimensional (3D) "linear-in-k" matrix element is derived using symmetries. Its two-dimensional (2D) adaptation requires a generalization of previous calculations. We get an expression for the scattering time which allows the determination of the order of magnitude of the "linear-in-k" deformation potential. In Sec. IV C, we discuss the proposed value for this new parameter assuming that the vicinity of the valleys relative to the zone edges is the key factor for this "linear-in-k" mechanism.

II. EXPERIMENTAL RESULTS

The experimental procedure for the realization of Si(111)/PEO polymer-electrolyte interfaces has been described in Refs. 9 and 14 and those relative to Si/[methanol+0.1M $LiClO_4$] electrolyte interfaces in the 180–290-K range (−95 to +15 °C) are in Ref. 14. Due to specific electrochemical factors, our meaningful density ranges above $\sim3\times10^{12}e^-/cm^2$. Because methanol is more reactive than acetonitrile, the maximum attainable density lies between 2.5×10^{13} and $4\times10^{13}e^-/cm^2$ depending upon the temperature.

We obtain the charge-potential $Q(V)$ relation of the accumulated interface toward negative ("cathodic") potentials from capacitance measurements. The conductance variation between the two contacts of the n-type-Si sample[9] yields the accumulation layer sheet conductance as a function of potential $\sigma_{acc}(V)$. Eliminating V, one gets the mobility in the 2D EG $\mu=|\sigma_{acc}/Q|=\mu(N_s,T)$ since $Q=eN_s$. Temperature scans allow the determination of the $\mu(T)$ relation at a given density N_s.

The dependence of the mobility upon N_s for our pretreated Si(111)/PEO interfaces ranges typically from $N_s^{-0.3}$ at "low" densities (3×10^{12}–$1.5\times10^{13}e^-/cm^2$) to about $N_s^{-0.7}$ at the highest densities (3×10^{13}–$4\times10^{13}e^-/cm^2$).[9] A similar behavior is obtained with Si/methanol-electrolyte interfaces.[14]

Figure 1 shows the mobility as a function of temperature at various densities between 1.0×10^{13} and $3.0\times10^{13}e^-/cm^2$, for Si/POE and Si/methanol interfaces in the 300–400-K and the 200–300-K ranges, respectively.[14] Data from Sato *et al.*[3] at a somewhat lower

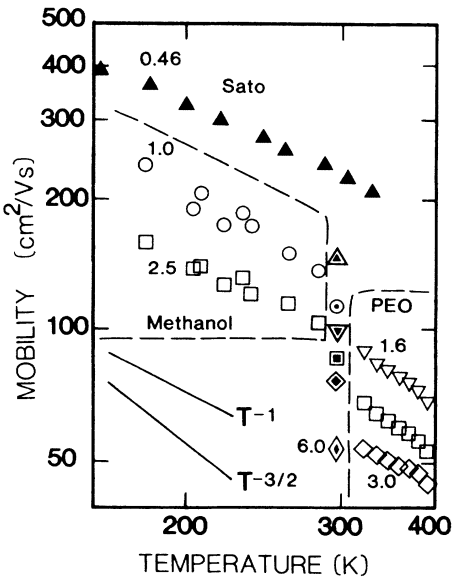

FIG. 1. Electron mobility as a function of temperature for various Si(111) electron layers at high concentrations: (▲), MOSFET inversion layer at $0.46\times10^{13}e^-/cm^2$, the highest density of Sato *et al.* (Ref. 3); (○, ▽, □, ◇), Si/PEO- and Si/methanol-electrolyte interfaces (our results) at 1.0, 1.6, 2.5, and $3.0\times10^{13}e^-/cm^2$, respectively; dotted symbols refer to Si/acetonitrile-electrolyte interfaces of Ref. 7 at densities given by the corresponding nondotted symbols above.

density are presented, as well as room-temperature data from Ref. 7 at corresponding densities. The overall dependence of the mobility as a function of temperature T ranges from T^{-1} for the methanol-electrolyte experiments to $T^{-3/2}$ for the PEO-electrolyte experiments at the densities shown here. At lower densities, the uncertainty on the exponent (less than 20% here) increases, since the mobility is the ratio of two smaller quantities, but nevertheless, we could not detect any indication in contradiction with a T^{-1}–$T^{-3/2}$ temperature dependence of the mobility. The order of magnitude of the measured mobilities is very low, especially for the Si/PEO interfaces (50–120 $cm^2/V\,s$), and does not exceed ~ 250 $cm^2/V\,s$ for the methanol electrolyte in the investigated range.

The methanol data are in agreement with the PEO data regarding the negative temperature dependence and the low order of magnitude of the mobility (100–250 $cm^2/V\,s$). In detail, the temperature dependence of the mobility is less steep (T^{-1} instead of $T^{-3/2}$) and its magnitude seems somewhat larger than that of Si/PEO interfaces. These minor discrepancies might be due to the chemical effects of methanol on the electrode surface[14,16] and we will not discuss them further. Finally, the most salient features of our mobility results are the $N_s^{-\alpha}T^{-\beta}$ dependence ($0.3<\alpha<0.7$ and $1.0<\beta<1.5$) and the low order of magnitude (50–250 $cm^2/V\,s$).

Both systems clearly confirm the predominance of phonon scattering in highly concentrated accumulation layers in the 200–400-K range, in the continuation of results obtained for Si/SiO_2 metal-oxide-semiconductor field-effect transistor (MOSFET) systems.[3,17] The order of magnitude of the mobility here is strikingly low, still lower than observed in MOSFET's.[3] As can be seen, this low order of magnitude is mainly due to the high density range investigated in our interfaces, since our data extrapolate fairly well those on MOSFET's.

The simplest theory for phonon-limited mobility in 2D EG is that for acoustic phonons from Kawaji[18] which predicts a $N_s^{-1/3}T^{-1}$ behavior of the mobility. Since intervalley phonons are known to be the major scattering source in bulk silicon at room temperature,[19,20] the actual temperature dependence of the mobility is expected to be somewhat steeper than T^{-1}, as observed in MOSFET's.[21] Hence, the $T^{-3/2}$ dependence of the Si/PEO data leads us to consider the theory of acoustic and intervalley phonon scattering in the case of a concentrated and possibly degenerate Si(111) 2D EG around room temperature.

III. THEORY OF ACOUSTIC AND INTERVALLEY PHONON SCATTERING IN Si(111) 2D EG

Highly accumulated electron layers combine possible degeneracy and efficient intervalley scattering. The Si(111) face may be treated within the one-subband approximation for two reasons: (i) most carriers lie in the fundamental subband, and (ii) in the case of the fundamental subband, intersubband coupling appears much weaker than its intrasubband counterpart, as will be explained later.

At the temperatures of interest here, the screening of acoustic phonons as computed from Refs. 22 and 23 is not important (less than 15%); since it is negligible for intervalley phonons, it will not be considered here. On the other hand, two important points have been misunderstood in the literature: the choice of intervalley phonons and the problem of degenerate statistics. We will discuss these two points in Secs. III A and III B, respectively.

A. Choice of intervalley phonons in Si(111) 2D EG

There are two types of relevant intervalley phonons in bulk silicon connecting either "noncoaxial" valleys (f type) or "coaxial" valleys (g type).[19,20] Both are *umklapp* phonons: the *umklapp* $\mathbf{q}_f$ and $\mathbf{q}_g$ phonon wave vectors are displayed in Fig. 2 showing three adjacent First Brillouin zones (FBZ) in the cubic centered reciprocal lattice. $\mathbf{q}_f$ and $\mathbf{q}_g$ involve, respectively, a $(2\pi/a)(1,1,1)$ and a $(2\pi/a)(2,0,0)$ reciprocal-lattice vector (a is the lattice parameter). Because $\mathbf{q}_f$ is only 12° off a (001) direction, Long has considered the phonon dispersion relation only along line ΓX and has gathered the energies of the various branches as 55 meV for f ($T_f=630$ K), while the g energy was taken within the most populated low-energy acoustic branches, at $\mathbf{q}_g \approx 0.3 k_{\Gamma X}$, as 16 meV ($T_g=190$ K).[20]

Ferry further remarked that the g phonon is forbidden at the zeroth order of the Harrison $\mathbf{k}\cdot\mathbf{p}$ expansion of the electron-phonon (e-ph) interaction.[15] He gave a more correct "first-order" expression[19] and the revised deformation potentials. He also applied this treatment to electron inversion layers but did not take into account the degeneracy properly. Roychoudhury and Basu pointed out a correct treatment of degeneracy[17] but made a criticizable choice for intervalley phonons: they neglected any component of the intervalley wave vector out of the interface plane; their phonons therefore differ from those of Long or Ferry (the fact that they were investigating the (100) face does not affect this point). This confused situa-

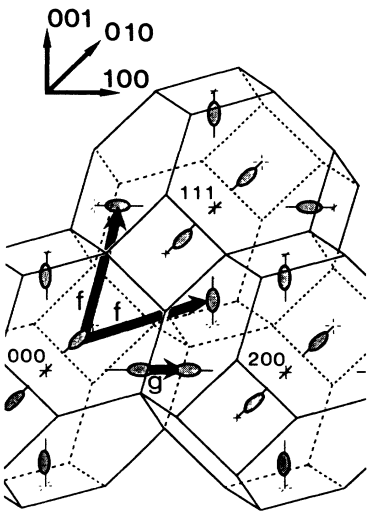

FIG. 2. Intervalley *umklapp* f and g phonons in the silicon reciprocal lattice; three adjacent first Brillouin zones are used. The valleys are represented by constant-energy ellipsoids.

tion leads us to first show in detail how and why Long's f and g phonons are still to be considered in the 2D case, and to further combine this choice with the correct treatment of degeneracy from Roychoudhury and Basu.[17]

Within the envelope-function framework,[1] the wave function of an electron in an accumulation (or inversion) layer reads

$$|\alpha m \mathbf{k}_{\|}\rangle = A^{-1/2} F_m(z) \exp(i\mathbf{k}_{\|}\cdot\mathbf{r}_{\|}) \exp(i\mathbf{K}_\alpha\cdot\mathbf{R}) \chi_\alpha(\mathbf{R}) , \tag{1}$$

where $\mathbf{R}\equiv(\mathbf{r}_{\|},z)$ is the space coordinate in and normal to the interface plane, respectively, A being its area. F_m is the envelope wave function in the mth subband of energy E_m of the αth valley located at $\mathbf{K}_\alpha$: the last two factors represent the usual Bloch function at the αth minimum and $\mathbf{k}_{\|}$ is the electron wave vector in the interface plane referred to the projection of $\mathbf{K}_\alpha$ in this plane. For the sake of simplicity, we assume an isotropic $E(\mathbf{k}_{\|})$ relation with the density-of-state mass m_D^*.

We deal with a phonon $\mathbf{q}\equiv(\mathbf{q}_{\|},q_z)$. The corresponding phonon perturbation is proportional to $\exp(i\mathbf{q}\cdot\mathbf{R})$ and its matrix element thus contains the factor

$$\langle \beta n \mathbf{k}'_{\|}|\exp(i\mathbf{q}\cdot\mathbf{R})|\alpha m \mathbf{k}_{\|}\rangle = \frac{1}{A}\int d^2\mathbf{r}_{\|}\int dz\, F_n^*(z)F_m(z)\exp\{i[(\mathbf{K}_\alpha-\mathbf{K}_\beta)_z+q_z]z\} \times\exp[i(\mathbf{k}_{\|}-\mathbf{k}'_{\|}+\mathbf{q}_{\|})\cdot\mathbf{r}_{\|}]\exp[i(\mathbf{K}_\alpha-\mathbf{K}_\beta)_{\|}\cdot\mathbf{r}_{\|}]\chi_\beta^*(\mathbf{R})\chi_\alpha(\mathbf{R}) , \tag{2}$$

and one reads a selection rule in the interface plane:

$$\mathbf{k}_{\|}-\mathbf{k}'_{\|}+\mathbf{q}_{\|}+(\mathbf{K}_\alpha-\mathbf{K}_\beta)_{\|}=\mathbf{g}_{\|} , \tag{3}$$

where $\mathbf{g}_{\|}$ is a vector of the reciprocal lattice of the surface. Along z, the integral is reduced by $F_mF_n^*$ to the interfacial region, so that no selection rule may apply *stricto sensu*.

The intravalley case ($\alpha=\beta$) classically yields the Fourier transform $I_{mn}(q_z)$ of the $F_mF_n^*$ product:

$$I_{mn}(q_z)=\int dz\,\exp(iq_zz)F_m(z)F_n^*(z) . \tag{4}$$

The width of $I_{mn}(q_z)$ hence characterizes an approximate selection rule in the z direction. Summing the z component of the phonons in the classical deformation-potential Hamiltonian, one obtains a rule for adapting a 3D matrix element $M_{\mathbf{q}}^{3D}$ to the 2D case:

$$|M_{\mathbf{q}_{\|}}^{2D}|^2=\left[\frac{V}{A}\right]\int_{-\infty}^{+\infty}\frac{dq_z}{2\pi}|I_{mn}(q_z)|^2\,|M_{\mathbf{q}}^{3D}|^2 . \tag{5}$$

Only matrix elements explicitly containing the electron wave vector $\mathbf{k}$ need a different treatment; this question will be addressed in Sec. IV. We may now compare the strength of intersubband ($m\neq n$) and intrasubband ($m=n$) couplings, taking $M_{\mathbf{q}}^{3D}$ as 1 in the above formula. In the case of the fundamental ($m=0$) and using self-consistent envelope functions, one obtains much larger strengths for $n=0$ (internal coupling) than for $n>0$ (coupling to excited subbands), typically in a ratio of 10 to 1.

The intervalley case ($\alpha\neq\beta$) yields in turn the expression

$$I_{mn}^{iv}(q_z)=\int dz\,F_n^*(z)F_m(z)\exp\{i[(\mathbf{K}_\alpha-\mathbf{K}_\beta)_z+q_z]z\} . \tag{6}$$

$I^{iv}(q_z)$ is identical with $I(q'_z)$ of Eq. (4) where $q'_z=q_z+(\mathbf{K}_\alpha-\mathbf{K}_\beta)_z$. This function will peak around $-q_z=(\mathbf{K}_\alpha-\mathbf{K}_\beta)_z$, with a characteristic width of the order of $\langle z\rangle^{-1}$, where $\langle z\rangle$ is the typical extent of the envelope wave functions. This form somewhat relaxes the selection rule in the z direction by allowing some spreading around the $(\mathbf{K}_\alpha-\mathbf{K}_\beta)_z$ 3D value. Since $(\mathbf{K}_\alpha-\mathbf{K}_\beta)_z$ is of the order of the FBZ and the $\langle z\rangle^{-1}$ spreading of the order of a small fraction of the FBZ, this spreading will be of little consequence on the relevant phonon energies and populations. Omitting the m,n indexes to focus on the fundamental subband approximation ($m=0$), Eq. (5) reduces to a simple form in the useful case of a q-independent matrix element:

$$|M^{2D}|^2=\left[\frac{V}{A}\right]J|M^{3D}|^2 , \tag{7}$$

with

$$J=\int\frac{dq_z}{2\pi}|I(q_z)|^2 . \tag{8}$$

To our knowledge, this general formulation for J [especially with $I^{iv}(q_z)\equiv I(q'_z)$ in the intervalley case] has not been given elsewhere before. Both J and its intervalley analog are of the order of $\langle z\rangle^{-1}$, as may be seen by replacing q_z by q'_z. We now use the approximate Fang-Howard wave function for the fundamental:[24]

$$F_0(z)=(\tfrac{1}{2}b^3z^2)^{1/2}\exp\left[\frac{-bz}{2}\right] ,$$
$$b=\left[\frac{33}{8}\frac{m_ze^2N_s}{\epsilon_r\epsilon_0\hbar^2}\right]^{1/3} , \tag{9}$$

where ϵ_r is the semiconductor dielectric constant, ϵ_0 the vacuum permittivity, and m_z the effective mass normal to the interface; $\hbar$ is the quotient of Planck's constant by 2π. Note that many parameters such as $\langle z\rangle=3b^{-1}$ vary like $N_s^{-1/3}$ because of Eq. (9). One gets the simple J value:[21]

$$J=3b/16 . \tag{10}$$

We have checked that this value does not differ from the values obtained by self-consistent calculations by more than 15%, and is, rather, lower than that. Acoustic phonons are a useful example for the computations that we have to carry out. We start from the well-known 3D ma-

trix element (+ for emission, − for absorption):[25]

$$|M^{3D}|_{\pm}=\left[\frac{D^2k_BT}{2\rho Vs_1^2}\right]^{1/2}, \tag{11}$$

where k_B is the Boltzmann constant, D is the (averaged) acoustic deformation potential, ρ the silicon volumic mass, s_1 the sound velocity in silicon, and V the crystal volume; the selection rule $\mathbf{k}'-\mathbf{k}\pm\mathbf{q}=0$ is applied to remove the $\mathbf{q}$ sum. It is independent of $\mathbf{q}$ so that one gets the 2D matrix element

$$|M^{2D}|_{\pm}^2=\frac{D^2k_BT}{2\rho As_1^2}J=\frac{3bD^2k_BT}{32\rho As_1^2}. \tag{12}$$

We calculate the corresponding scattering time $\tau^{2D,ac}$ using the classical Fermi golden rule, the Boltzmann equation for elastic collisions,[17,22,25] and the energy-independent density of states (density-of-state mass m_D^*). We get an expression independent of energy and degeneracy:

$$\frac{1}{\tau^{2D,ac}}=\left[\frac{3bD^2k_BTm_D^*}{16\rho s_1^2\hbar^3}\right]. \tag{13}$$

The squared matrix element for intervalley-phonon scattering has been given by Ferry[21] and Roychoudhury and Basu[17] for the f zero-order mechanism:

$$|M^{2D,f}|^2=\left[\frac{D_{\text{opt}}^2\hbar}{2\rho A\omega_q}\right]\times J[n_q\delta(E(\mathbf{k}_\parallel)-E(\mathbf{k}'_\parallel)+\hbar\omega_q)+(n_q+1)\delta(E(\mathbf{k}_\parallel)-E(\mathbf{k}'_\parallel)-\hbar\omega_q)], \tag{14}$$

where $\mathbf{q}=\mathbf{K}_\beta-\mathbf{K}_\alpha$, ω_q is the phonon pulsation, and D_{opt}, the relevant deformation potential, is so called because the f phonon is essentially optical. For the g phonon, some additional indications will be given in Sec. IV: as mentioned above, the 3D matrix element explicitly contains the electron wave vectors with respect to their minima—and not only the phonon wave vector—so that Eqs. (4) and (5) are not valid in principle; Ferry's notations of Ref. 21 may be misleading on this point. However, because of our pedagogical purpose and the very small relative weight of the g phonon, in this section we will use the expressions directly derived from those of Ferry for the scattering time after the issue of degeneracy is clarified.

B. Treatment of degeneracy

Ferry has given an expression for the nondegenerate case. As stated in Ref. 17, in the treatment of collisions randomizing isotropically the final velocity such as intervalley-phonon scattering, the collision term of the Boltzmann equation gives the following expression for the scattering rate in the 2D case:

$$\frac{1}{\tau^{2D}}=\frac{A}{(2\pi)^2}\int d^2\mathbf{k}'\,P(\mathbf{k},\mathbf{k}')\left[\frac{1-f_0(\mathbf{k}')}{1-f_0(\mathbf{k})}\right], \tag{15}$$

where $P(\mathbf{k},\mathbf{k}')$ is the transition probability as given by the Fermi golden rule, and $f_0(\mathbf{k})$ the equilibrium Fermi-Dirac distribution function in reciprocal space. The denominator $[1-f_0(\mathbf{k})]$ is often omitted although it stems directly from the application of the detailed balance principle.

Taking into account the choice made in Sec. III A for intervalley phonons, we get the relevant expression for the scattering rate due to intervalley-phonon scattering in a variably degenerate Si(111) accumulation layer:

$$\frac{1}{\tau^{2D,f}(E)}=\left[\frac{m_D^*D_{\text{opt}}^2}{2\rho\hbar^2\omega_q}\right]J\left[n_q\frac{1-f_0(E+\hbar\omega_q)}{1-f_0(E)}+(n_q+1)\frac{1-f_0(E-\hbar\omega_q)}{1-f_0(E)}\Theta(E-\hbar\omega_q)\right] \tag{16}$$

for the f "zeroth-order" phonon, where Θ is the Heaviside unit-step function [$\Theta(x)=0$ if $x<0$ and $\Theta(x)=1$ if $x>0$]. From Ref. 21, we derive the following scattering rate for the g first-order phonon in the degenerate case using the D_1 deformation potential (see also Sec. IV):

$$\frac{1}{\tau^{2D,g}(E)}=\left[\frac{m_D^{*2}D_1^2}{\hbar^4\rho\omega_q}\right]J\left[n_q(2E+\hbar\omega_q)\frac{1-f_0(E+\hbar\omega_q)}{1-f_0(E)}+(n_q+1)(2E-\hbar\omega_q)\frac{1-f_0(E-\hbar\omega_q)}{1-f_0(E)}\Theta(E-\hbar\omega_q)\right]. \tag{17}$$

Using Eq. (12) for the acoustic scattering time, we get the energy-independent scattering time by adding the various contributions and by using the 2D average:

$$\langle\tau\rangle=\left[\int dE\,E\frac{\partial f_0(E)}{\partial E}\left[\sum_{i=ac,f,g}[\tau^{2D,i}(E)]^{-1}\right]^{-1}\right]\left[\int dE\,E\frac{\partial f_0(E)}{\partial E}\right]^{-1}. \tag{18}$$

The mobility is $\mu=e\langle\tau\rangle/m_c^*$, m_c^* being the conductivity mass. For numerical computations, we use the values from Refs. 1 and 21 (see Table I).

The resulting mobility is plotted versus temperature between 20 and 500 K at densities scaled as powers of 2 from $0.125\times10^{13}e^-/\text{cm}^2$ to $16\times10^{13}e^-/\text{cm}^2$ on the $\log(\mu)$-$\log(T)$ plot of Fig. 3. Experimental data of Sec. II for the Si/PEO and Si/methanol interfaces are shown as rectangles.

As can be seen, the theory overestimates the mobility by a factor of 6–9. Within the above framework, reducing this discrepancy without changing the deformation

TABLE I. Numerical data used for the computations.

Bulk silicon data	
Volumic mass	$\rho=2.33\times10^{3}$ kg m^{-3}
Sound velocity (this is an optimized average)	$s_l=9.00\times10^{3}$ m s^{-1}
Electron mass	$m_0=9.05\times10^{-31}$ kg
Density-of-state mass	$m_D^*=0.32m_0$
Conductivity mass	$m_C^*=0.30m_0$
$-e/m_C^*$ ratio	$-e/m_C^*=5.89\times10^{11}$ C kg^{-1}
Uniaxial deformation potential	$D=9$ eV
Si(111) face	
Parallel effective masses	$m_1=0.71m_0$, $m_2=0.19m_0$
Perpendicular effective mass	$m_3=m_z=0.26m_0$
Density-of-state effective mass (parallel)	$m_D^*=0.367m_0$
Conductivity effective mass (parallel)	$m_C^*=0.30m_0$
Long parameters as revised by Ferry	
Intervalley f phonon ("zero order")	$T_f=630$ K, $D_{\text{opt}}=9\times10^{10}$ eV/m
Intervalley g phonon ("first order")	$T_g=190$ K, $D_l=5.6$ eV

potentials seems difficult. Effects such as screening, which has not been taken into account, increase the predicted mobility. The use of the "exact" self-consistent envelope wave function instead of the Fang-Howard approximation used here would lower the predicted mobility because it tends to increase the integral J of Eq. (8), but by no more than 15%. Hence the unsatisfactory situation quoted for classical MOSFET inversion layers[1] becomes still worse at the higher densities of our very-high-density accumulation layers. The use of specific "interface" phonon modes (surfons) has been investigated by Ezawa and co-workers[4] in the early 1970's without much success. Other authors[5,6] suggested later that the deformation potential would be enhanced near the surface, but they did not give good reasons or confirm their prediction. Hence, in the following we are attempting to suggest a suitable mechanism for such a scattering enhancement.

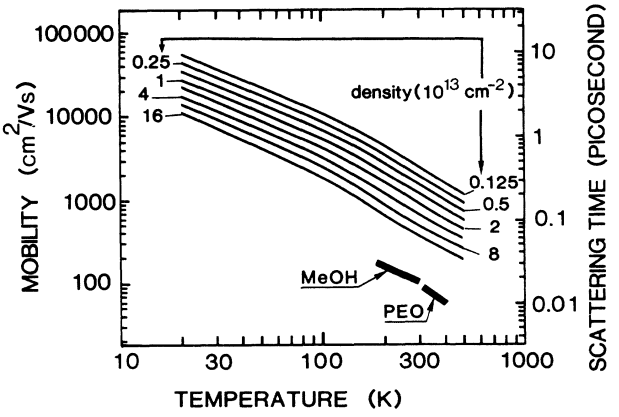

FIG. 3. Computed electron scattering time and mobility of electrons limited by acoustic and intervalley phonon scattering as a function of temperature for densities scaling as powers of two from $0.125\times10^{13}e^-$/cm^2 to $16\times10^{13}e^-$/cm^2 in a Si(111) accumulation layer. Our data on Si/PEO- and Si/methanol-electrolyte interfaces at $2.5\times10^{13}e^-$/cm^2 are shown as rectangles.

IV. SCATTERING MECHANISM OF HIGHER ORDER IN k·p AT HIGHER DENSITIES

The trend of decreased mobility with increasing electron density strongly suggests the existence of a mechanism specific to these large electronic concentrations.

One might think first that the large electric field induces some kind of additional scattering mechanism by changing locally the nonpolar nature of silicon, thus making a layer of $Si^{+\delta}$-$Si^{-\delta}$ silicon analogous to III-V compounds. In this layer, polar-optical phonon and piezoelectric scattering might become noticeable.[26] It can be easily predicted that the resulting mobility would depend on N_s too strongly to fit any part of the experimental data while its predicted order of magnitude, although more difficult to assess, would still be too high.

A more direct consequence of the high densities is the increased occupancy of the reciprocal space (RS) around the valley minima so that the deformation-induced behavior of the bands in the vicinity of the minima can affect the conduction electrons. It is simpler first to discuss this matter in the case of bulk silicon.

A. Intuitive formulation

The effect of strain on the band structure is usually described by the deformation potential D: there is a local shift $\delta E_c=D\Delta$ of the energy of the band edge proportional to the local dilation Δ. If electrons do populate a significant region around minima, we might have to allow D to become wave-vector dependent. A simple way to achieve this to a first-order approximation is to assume a shift δE_c proportional to k, the wave vector relative to the minima, with some constant D_k:

$$\delta E_c=(D_0+D_k k)\Delta \ . \tag{19}$$

This shift of the band edge, linear in k, obviously corresponds to a displacement δK of the minima, as suggested in Fig. 4. Using the effective mass m^*, one has

$$D_k\Delta=\hbar^2\delta K/m^* \ . \tag{20}$$

The additional mechanism proposed here may thus be seen as a deformation-induced displacement of the minima locations in the reciprocal space, in addition to the uniform band-edge shift described by the usual deformation-potential mechanism. However, the above expression is not a rigorous perturbation Hamiltonian. A more proper formulation of this mechanism will now be given.

B. Harrison k·p expansion of *e*-ph interaction in nonpolar semiconductors; Origin of the "linear-in-*k*" mechanism

Harrison[15] has formulated the matrix elements for *e*-ph scattering in nonpolar centrosymmetric semiconductors (e.g., Si) using the **k·p** expansion: the matrix element of the phonon perturbation between two electronic states $\mathbf{k},\mathbf{k}'$, counted relative to their respective minima $\mathbf{K}_\alpha$ and $\mathbf{K}_\beta$ reads

$$M^{3D}_{\alpha\mathbf{k}\beta\mathbf{k}'}=\int_C d^3\mathbf{r}\,\chi^*_{\mathbf{K}_\beta+\mathbf{k}'}\chi_{\mathbf{K}_\alpha+\mathbf{k}}R\,\mathbf{e}_\mathbf{q}\cdot\nabla_\mathbf{r}\mathcal{V}\ , \tag{21}$$

where C is the two-atom unit cell where the $\mathbf{r}$ space variable runs, the χ's are the periodic parts of the Bloch wave functions of the $\mathbf{k},\mathbf{k}'$ states in the αth and βth valleys, $\mathbf{e}_\mathbf{q}$ is a unit vector describing the atomic displacement induced by the phonon whose wave vector is $\mathbf{q}$. The selection rule $\mathbf{k}\pm\mathbf{q}-\mathbf{k}'=\mathbf{0}$ has been used previously and the phonon amplitude (or occupation number) is dropped. R is a function describing the symmetries of the phonon mode (acoustical or optical) and having additional crystal symmetries (see Ref. 15 for details); $\mathcal{V}$ is the potential of crystal atoms.

We must consider all the bands and add a band index i to the wave functions. We assume $\hbar=m^*=1$ for convenience and drop the valley index (α,β); expressions of interest for the intervalley case (Sec. III) will be mentioned. In the **k·p** expansion, one of the $\chi^i_{\mathbf{K}+\mathbf{k}}$ is expanded on the set of the $\chi^j_\mathbf{K}$ wave functions, using the perturbation operator $\mathbf{k}(-i\nabla_\mathbf{r}+\mathbf{K})$ at first order in $\mathbf{k}$:

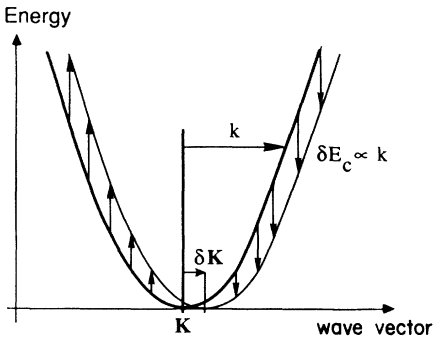

FIG. 4. First-order effect of strain on band structure at a band minimum **K** far from zone center: instead of an even shift of the band everywhere around the minimum, the minimum location is shifted by $\delta\mathbf{K}$ corresponding to a k-dependent shift of the band edge (vertical arrows).

$$\chi^i_{\mathbf{K}+\mathbf{k}}=\chi^i_\mathbf{K}+\sum_{j\,(\neq i)}\frac{H_{ji}(\mathbf{k})}{E_i-E_j}\chi^j_\mathbf{K}+\sum_{j\,(\neq i),\ l\,(\neq i)}\frac{H_{lj}(\mathbf{k})H_{ji}(\mathbf{k})}{(E_i-E_j)(E_i-E_l)}\chi^l_\mathbf{K}+\cdots\ , \tag{22}$$

where

$$H_{ji}(\mathbf{k})=-i\mathbf{k}\cdot\int_C d^3\mathbf{r}\,\chi^{j*}_\mathbf{K}\nabla_\mathbf{r}\chi^i_\mathbf{K}\ .$$

Successive orders in $\mathbf{k}$ thus appear in $M_{\mathbf{k}\mathbf{k}'}$. For acoustical phonons, a symmetrical R_{ac} function is used and the zero-order term:

$$M^{3D(0)}_{\mathbf{k}\mathbf{k}'}=\mathbf{e}_\mathbf{q}\cdot\int_C d^3\mathbf{r}\,\chi^{i*}_\mathbf{K}\chi^i_\mathbf{K}R_{ac}\nabla_\mathbf{r}\mathcal{V} \tag{23}$$

vanishes: this is obvious at the zone center, where the $\chi^i_\mathbf{K}$'s may be taken as real and of a given symmetry (even or odd), whereas $\nabla_\mathbf{r}\mathcal{V}$ is odd. Similar arguments far from the zone center require a more careful use of the inversion operator.[15] The first-order term is also obtained through the use of this operator, restricting the summation to the half-cell $C/2$. The R_{opt} function to be used for optical phonons changes sign under inversion, whereas R_{ac}, its acoustical counterpart, does not. The result reads

$$M^{3D(1)}_{\mathbf{k}\mathbf{k}'}=\sum_{j\neq i}\left[\mathbf{e}_\mathbf{q}\cdot\int_{C/2}d^3\mathbf{r}\,(\chi^{i*}_\mathbf{K}\chi^j_\mathbf{K}\pm\text{c.c.})R\nabla_\mathbf{r}\mathcal{V}\right]\times\left[\frac{-i}{E_i-E_j}(\mathbf{k}\pm\mathbf{k}')\cdot\int_C d^3\mathbf{r}\,\chi^{i*}_\mathbf{K}\nabla_\mathbf{r}\chi^j_K\right], \tag{24}$$

with the plus sign standing for optical phonons and the minus sign for acoustical phonons. In the latter case, one gets the usual matrix element proportional to $\mathbf{k}-\mathbf{k}'=\mathbf{q}$. The optical case, restoring the omitted valley indexes, corresponds to the "first-order" g-type intervalley phonon, forbidden at zero order as pointed out by Ferry. It contains $(\mathbf{k}+\mathbf{k}')$ explicitly and cannot therefore be expressed exactly with $\mathbf{q}$ only. Hence, the use of Eqs. (4)–(6) above is not correct in principle for this matrix element; this question will be addressed in Sec. IV C. Note also that Ferry's treatment[19] neglects the $\mathbf{k}\cdot\mathbf{k}'$ term appearing in $|M|^2$. This approximation has little effect on the result and is also justified by the fact that the g phonon has both acoustical and optical components noticeable since it lies at a low-symmetry point of the FBZ, hence a further reduction of the small $\mathbf{k}\cdot\mathbf{k}'$ contribution.

Now, we are interested in the second-order terms, one order more than the usual matrix element. We restrict ourselves to acoustical phonons. A first part comes from the first-order terms in the $\mathbf{k}$ and $\mathbf{k}'$ states; it contains terms such as

$$\sum_{j\,(\neq i),\ l\,(\neq i)} \left[\mathbf{e_q}\cdot\int_{C/2} d^3\mathbf{r}\,(\chi^{j*}_{\mathbf{K}}\chi^{l}_{\mathbf{K}} - \text{c.c.})R_{\text{ac}}\nabla_{\mathbf{r}}\mathcal{V} \right] \times \left[\frac{1}{(E_i-E_l)}\mathbf{k}\cdot\int_C d^3\mathbf{r}\,\chi^{l*}_{\mathbf{K}}\nabla_{\mathbf{r}}\chi^{i}_{\mathbf{K}} \right] \times \left[\frac{1}{(E_i-E_j)}\mathbf{k}'\cdot\int_C d^3\mathbf{r}\,\chi^{j*}_{\mathbf{K}}\nabla_{\mathbf{r}}\chi^{i}_{\mathbf{K}} \right] , \tag{25}$$

i.e., terms in $\mathbf{k}_\mu\cdot\mathbf{k}'_\nu$. Similar terms are also obtained between the zero- and second order of each state, but yield instead a contribution of the type $\mathbf{k}_\mu^2-(\mathbf{k}'_\nu)^2$. It may be seen by taking the complex conjugate that the result changes sign when inverting $\mathbf{k}$ and $\mathbf{k}'$.

Hence, the relevant higher-order matrix element is obtained by substituting the $(\mathbf{k}-\mathbf{k}')$ term of the usual acoustical-phonon matrix element by a quadratic form in $(\mathbf{k},\mathbf{k}')$, antisymmetrical in $(\mathbf{k},\mathbf{k}')$. The 36 coefficients of its representative matrix may be reduced to only 15 using the form symmetry and the $(\mathbf{k},\mathbf{k}')$ antisymmetry. However, group theory is required to predict which of the H_{ij} vanish due to symmetry. Since the conduction-band valleys in silicon lie at a low-symmetry point, one may expect that a sufficient part of these terms will not vanish so that a noticeable second-order term is expected. Finally, an expression such as

$$M_{\mathbf{kk}'} \propto D_k(\mathbf{k}-\mathbf{k}')\cdot(\mathbf{k}+\mathbf{k}') = D_k\mathbf{q}\cdot(\mathbf{k}+\mathbf{k}') , \tag{26}$$

where D_k is an appropriate constant, meets the symmetry requirements and describes satisfactorily a "linear-in-k" effect similar to that inferred in Sec. IV A.

Two further approximations ultimately simplify the treatment.

(i) Only the isotropic part of the matrix element is used, as for the "first-order" treatment of the g-type intervalley phonon:[19]

$$|M| \propto D_k|\mathbf{q}|[\mathbf{k}^2+(\mathbf{k}')^2]^{1/2} . \tag{27}$$

(ii) We temporarily ignore the coherent nature of the higher-order perturbation, i.e., the fact that it has *a priori* a given phase relative to the usual $\delta E_c = D\Delta$ perturbation.

Table II gives a summary of the expressions of the various terms of the e-ph interaction for orders 0–2 in $\mathbf{k}\cdot\mathbf{p}$.

C. 2D treatment of the higher-order mechanisms

Equation (27) above contains explicitly $\mathbf{k}$ and $\mathbf{k}'$, and not only $\mathbf{q}$. Also the first-order interaction of the g phonon as deduced from Eq. (24) gives a term quite similar to Eq. (26) from this point of view, or Eq. (27) if the same isotropic approximation is made. For such cases, we cannot use the framework of Sec. III as such. Instead, we must come back to Eq. (2) for the general 2D matrix element, express the envelope wave-function $F(z)$ on the plane-wave basis $\exp(ik_z z)$, and sum over k_z before summing over space coordinates. We restrict the discussion to the fundamental subband for clarity. We make use of the Fourier transform of $F(z)$:

$$\Phi(k_z) = \int dz\,\exp(-ik_z z)F(z) . \tag{28}$$

Out of the three vectors $\mathbf{k},\mathbf{k}',\mathbf{q}$, we can use immediately the $\mathbf{k}'_\parallel = \mathbf{k}_\parallel \pm \mathbf{q}_\parallel$ selection rule of Eq. (3) so that we are left with the nonredundant variables $\mathbf{k},\mathbf{k}',q_z$ before summation; whenever $\mathbf{q}$ will appear in the following, it will stand for $(\mathbf{k}'_\parallel-\mathbf{k}_\parallel, q_z)$ and only the nonredundant variables $(\mathbf{k},\mathbf{k}', q_z)$ will be used in the subscript for the matrix element. One obtains the following generalization of Eq. (5) of Sec. III:

TABLE II. Schematic form of the matrix elements of the electron-phonon interaction for acoustical and optical phonons for orders 0–2 of the $\mathbf{k}\cdot\mathbf{p}$ expansion of the periodic part of the electronic Bloch wave functions.

Phonon	Acoustical	Optical	Remarks
Relative displacement of the atoms in the elementary unit cell	In phase at zero order in q (center of FBZ)	In opposition at zero order in q (center of FBZ)	The phase relation is more complicated at FBZ edge
Electronic transition	Intravalley ($\mathbf{k}\rightarrow\mathbf{k}'$)	Intravalley ($\mathbf{k}\rightarrow\mathbf{k}'$) or intervalley ($\mathbf{K}_\alpha+\mathbf{k}\rightarrow\mathbf{K}_\beta+\mathbf{k}'$)	
Order in $\mathbf{k}$	Expression of $M_{\mathbf{kk}'}$ $\{k\equiv[k^2+(k')^2]^{1/2}\}$		Isotropic approximation
0	zero	$D_{\text{opt}}\equiv D_0$	optical phonon f
1	Dq (usual deformation potential)	$D_1 k$	optical phonon g
2	$D_k kq$ (displacement of the minimum)	$[D_2 k^2]$	"linear-in-k" mechanism

$$|M^{2D}_{\mathbf{k}_\parallel \mathbf{k}'_\parallel}|^2=\frac{V}{A}\int_{-\infty}^{+\infty}\frac{dq_z}{2\pi}\left|\int dz\int\frac{dk'_z}{2\pi}\Phi^*(k'_z)\int\frac{dk_z}{2\pi}\Phi(k_z)\exp[i(k_z-k'_z+q_z)z]M^{3D}_{\mathbf{k}\mathbf{k}'q_z}\right|^2 . \tag{29}$$

Fortunately, this may be simplified using the relation $\int dz\,\exp[i(k_z-k'_z+q_z)z]=2\pi\delta(k_z-k'_z+q_z)$; this Dirac function allows the suppression of the k'_z integral, substituting $\Phi^*(k'_z)$ by $\Phi^*(k_z+q_z)$ and $\mathbf{k}'$ by $\mathbf{k}+\mathbf{q}$:

$$|M^{2D}_{\mathbf{k}_\parallel \mathbf{k}'_\parallel}|^2=\left[\frac{V}{A}\right]\int_{-\infty}^{+\infty}\frac{dq_z}{2\pi}\left|\int\frac{dk_z}{2\pi}\Phi^*(k_z+q_z)\Phi(k_z)M^{3D}_{\mathbf{k}\mathbf{k}'_\parallel q_z}\right|^2 . \tag{30}$$

We split M^{3D} into a $\mathbf{q}$-dependent part $C(\mathbf{q})(n_\mathbf{q}+\frac{1}{2}\pm\frac{1}{2})^{1/2}$ and a $\mathbf{k}$-dependent part $R(\mathbf{k},\mathbf{k}')$ which would have been 1 in the cases seen above:

$$M^{3D}_{\mathbf{k}\mathbf{k}'q_z}=C(\mathbf{q})(n_\mathbf{q}+\tfrac{1}{2}\pm\tfrac{1}{2})^{1/2}R(\mathbf{k},\mathbf{k}') . \tag{31}$$

In the two cases of interest here, $R(\mathbf{k},\mathbf{k}')=[\mathbf{k}^2+(\mathbf{k}')^2]^{1/2}$ is the same. The "linear-in-k" mechanism has the same $\mathbf{q}$-dependent part $C(\mathbf{q})(n_\mathbf{q}+\frac{1}{2}\pm\frac{1}{2})$ as acoustic phonons if one uses D instead of D_k:

$$|C(\mathbf{q})|(n_\mathbf{q}+\tfrac{1}{2}\pm\tfrac{1}{2})^{1/2}=\left[\frac{D_k^2 k_B T}{2\rho V s_1^2}\right]^{1/2} . \tag{32}$$

On the other hand, the first-order mechanism (g phonon) makes use of a constant $|C(\mathbf{q})|$:

$$|C(\mathbf{q})|=\left[\frac{D_1^2\hbar}{2\rho V\omega_\mathbf{q}}\right]^{1/2} . \tag{33}$$

From Eqs. (30) and (31), we see that the treatment of Sec. III is modified essentially for the $\mathbf{k}$-dependent part of the matrix element: the $\mathbf{q}$-dependent part is taken out of the square modulus of Eq. (30) and plays the role of the 3D matrix element in Eq. (5) of Sec. III. The integral remaining in the square modulus is also similar to $I(q_z)$, the Fourier transform of $|F|^2$, but this integral now contains the additional $\mathbf{k}$-dependent part $R(\mathbf{k},\mathbf{k}')$ of the matrix element; it is therefore logical to call it $I_k(q_z)$:

$$I_k(q_z)=\int\frac{dk_z}{2\pi}\Phi^*(k_z+q_z)\Phi(k_z)R(\mathbf{k},\mathbf{k}+\mathbf{q}) . \tag{34}$$

The calculation of $I_k(q_z)$ is made in Appendix A in the case of the Fang-Howard wave function, for elastic or inelastic scattering; in the latter case, one simply replaces the $k_\parallel^2$ factor of the former by $(k_\parallel^2+k'^2_\parallel)/2$ so that we need deal with only the elastic case in the following; the computation results in a complex expression which is analytical but somewhat involved. It is possible to find a simple approximation of the square modulus $|I_k(q_z)|^2$ in terms of the product of $|I(q_z)|^2$ and an expression bilinear in $k_\parallel^2$ and q_z^2. It avoids the numerical integration of $|I_k(q_z)|^2$, the last step to obtain the 2D matrix element, as confirmed in Appendix A. It eventually results in an excellent approximation of $J_k=\int(dq_z/2\pi)|I_k(q_z)|^2$, the equivalent of J in Sec. III, but using $I_k(q_z)$ instead of $I(q_z)$; this expression may be written as

$$J_k=\int_{-\infty}^{+\infty}\frac{dq_z}{2\pi}|I_k(q_z)|^2\approx b(A_0b^2+A_1k_\parallel^2) , \tag{35}$$

where the constants are $A_0=0.0784$ and $A_1=0.426$ (see Appendix A). The scattering time for our new higher-order mechanism taken separately is simply obtained by substituting the term JD^2 by $J_kD_k^2$ in Eq. (11) of the scattering time for acoustic phonons:

$$\frac{3b}{16}D^2\to b(A_0b^2+A_1k_\parallel^2)D_k^2 . \tag{36}$$

We may therefore define the scattering time $\tau^{2D,k}(E)$ of this mechanism (taken separately from the usual deformation-potential mechanism) for electrons at energy E within the plane:

$$\frac{1}{\tau^{2D,k}(E)}=\frac{k_BTm_D^*b}{\rho\hbar^3s_1^2}D_k^2\left[A_0b^2+A_1\frac{2m_D^*E}{\hbar^2}\right] . \tag{37}$$

A similar treatment is applied to obtain the scattering rate due to the first-order g phonon in Appendix B, starting from Eq. (16) since the collision is no more elastic; the result, given for the absorption ($\bar\tau_+$) and emission ($\bar\tau_-$) contributions independently ($\bar\tau^{-1}=\bar\tau_+^{-1}+\bar\tau_-^{-1}$), reads

$$\frac{1}{\bar\tau_\pm^{2D,g}(E)}=\frac{m_D^*b}{2\rho\hbar^2\omega_\mathbf{q}}D_1^2\left[A_0b^2+\frac{A_1m_D^*}{\hbar^2}(2E\pm\hbar\omega_\mathbf{q})\right]\times(n_\mathbf{q}+\tfrac{1}{2}\pm\tfrac{1}{2})\frac{1-f_0(E\pm\hbar\omega_\mathbf{q})}{1-f_0(E)} ; \tag{38}$$

as explained in Appendix B, the difference with Eq. (17) of Sec. III is noticeable, but the relatively small contribution of the g phonon makes it barely detectable, so that we do not discuss it further.

We may now discuss Eq. (37) for the "linear-in-k" mechanism: the Tb^3 term yields a $N_s^{-1}T^{-1}$ dependence of the mobility μ, whereas the TbE term yields a $N_s^{-1/3}T^{-2}$ behavior in the nondegenerate regime and a $N_s^{-4/3}T^{-1}$ behavior in the degenerate regime. This last term is just the one that we would have found upon simple substitution of D by $D_kk\propto D_k(E)^{1/2}$. All these exponents are compatible with experimental results, keeping in mind that we are near the borderline of the degenerate domain ($N_s^{-1/3}T^{-2}\to N_s^{-4/3}T^{-1}$). From Eq. (37), the $\mu(N_s)$ relation should also become steeper at the higher densities, whereas the $\mu(T)$ relation should be less steep when increasing the degeneracy; for example, by increasing N_s or decreasing T. Experimental results exhibit a systematically steeper $\mu(N_s)$ relation toward higher densities. However, the slope barely reaches -0.7 instead of the steeper -1 predicted slope.[9] As for the $\mu(T)$ relation, its softening at higher densities is more difficult

to assess because only a small effect is expected in the experimental temperature range. However, the data seem to exhibit such a trend, in agreement with theory.

We can finally improve the agreement with theory by including the term of crossed interference between our new mechanism and the usual deformation-potential mechanism. Indications on this additional term are given in Appendix C. The main result therein is easy to explain: this crossed term reads $\int (dq_z/2\pi) 2\mathrm{Re}[I(q_z)I_k(q_z)]$. Its behavior as a function of $k_\parallel^2 \propto E$ is therefore similar to that of $(JJ_k)^{1/2}$, i.e., (constant $+E)^{1/2}$. At high energy, this crossed term yields a $N_s^{-1/3}T^{-3/2}$ behavior of the mobility in the nondegenerate regime and a $N_s^{-5/6}T^{-1}$ behavior in the degenerate regime. At low energy, it yields a $N_s^{-2/3}T^{-1}$ behavior. These trends are quite close to the experimental ones. This good behavior as well as the low values of the mobility suggest the presence of a constructive crossed term, which will now be assumed.

Figure 5(a) shows the result of computations including this new mechanism and a constructive crossed term in addition to the intravalley and intervalley mechanisms of Sec. III. The value of the constant D_k has been adjusted

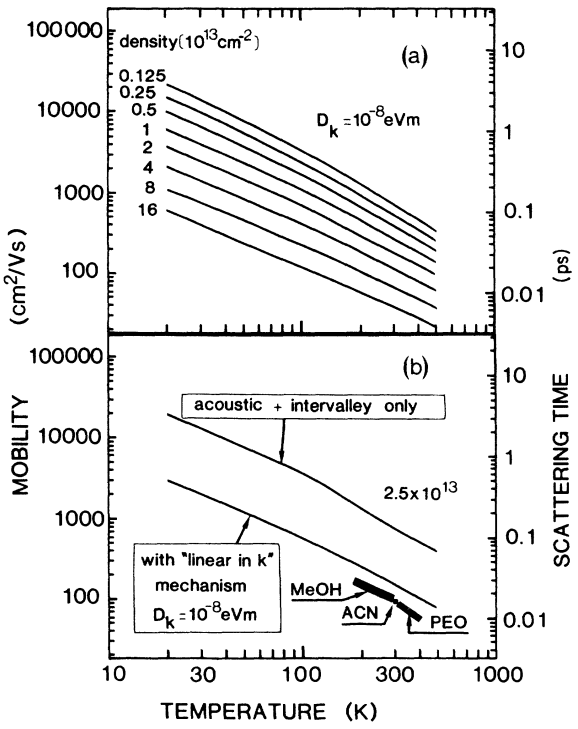

FIG. 5. (a) Computed scattering time and mobility of electrons as a function of temperature for various densities in a Si(111) accumulation layer including the new "linear-in-k" mechanism in addition to the acoustic and intervalley ones of Fig. 3. We use the same densities as in Fig. 3. (b) Comparison between the predicted mobility as a function of temperature due to acoustic and intervalley phonons (upper curve) or including the "linear-in-k" mechanism (lower curve) and the experimental data at $2.5\times10^{13}e^-/\mathrm{cm}^2$. Our results on Si/PEO- and Si/methanol-electrolyte interfaces are indicated as PEO and MeOH, whereas those of Ref. 7 at room temperature on Si/acetonitrile-electrolyte interfaces are indicated by ACN.

to 10^{-8} eV m in order to fit the experimental data. As expected, this new mechanism has a rather poor efficiency at low densities and temperatures, just as it has a negligible effect on the 3D mobility, but it greatly overcomes the usual acoustic mechanism at the highest densities for any temperature. Notice that a sizeable contribution comes from the crossed term. The absolute mobility values are in correct agreement with the experiments, as may be seen in Fig. 5(b), where we have chosen only the $2.5\times10^{13}e^-/\mathrm{cm}^2$ density value in order to compare to our experiments and those of Ref. 7 as well as to the previous result of Sec. III: it may be seen how inadequate the latter is.

Our theoretical prediction seems fully compatible with the observed $\mu \propto T^{-3/2}$ dependence, the experimental uncertainties suitably accounting for the residual differences. This new mechanism is thus altogether satisfactory and has seemingly never been contradicted by the experiments.

D. Relation with silicon band structure

The value of the usual deformation-potential D has been cross checked with values obtained from different experiments.[20,27,28] Such a check is more difficult for the quantity D_k introduced here. However, we may combine this value with an adequate wave vector to carry out a comparison with the known D and D_{opt} values of acoustical and intervalley scattering. In particular, due to the degeneracy, the kinetic energy perpendicular to the interface can reach about 100 meV, this is the energy of electrons at the X zone edge within the parabolic approximation. Such a region is very likely to exhibit enhanced effects of strain on band energy: when bands cross at a high-symmetry point such as X, any uniaxial strain is expected to lift the degeneracy; in the case of a perturbation of, say, first order, the gap that opens at the anticrossing point is one order less relative to the perturbation than the band displacement far from this point. Hence, a much larger zeroth-order effect than elsewhere is expected at points such as X. We have seen that the interaction of electrons with acoustic phonons is of first order with respect to the $\mathbf{k}\cdot\mathbf{p}$ expansion. It should therefore induce a zeroth-order effect near degenerate points, that is, of the same order of magnitude as the matrix element of an optical phonon.

An adequate wave vector for our comparison is thus the one going from the valley minima at $0.85k_{\Gamma X}$, the origin of the $\mathbf{k}\cdot\mathbf{p}$ expansion, to the X point, where we expect enhanced effects. The magnitude of this vector is $q_g/2 \sim 0.17\times10^{10}$ m^{-1}. Let us now compare the coupling constant of a typical zeroth-order element such as $D_{\mathrm{opt}} = 9\times10^{10}$ eV/m or of a first-order element such as $D = 9$ eV to our second-order element D_k. Using $q_g/2$, we get $D_{\mathrm{opt}}/(q_g/2)^2 = 3.1\times10^8$ eV m in the first case and $D/(q_g/2) = 0.53\times10^8$ eV m in the second case. It is seen that our proposed value $D_k = 10^8$ eV m takes place reasonably well in this range. This leads us to assume that the proximity of the zone edge enhances the second-order element to a magnitude similar to those of the first-order and zeroth-order elements. To substantiate

our point of view, we have studied the band structure of silicon near the X point.[29,30]

We have computed and plotted constant-energy surfaces in this region, using the pseudopotential method of Cohen and Bergstresser.[29] Figure 6 presents a 3D view of the surface whose energy is ~ 170 meV above the X-point energy, revealing significant features. The surface corresponding to the Δ_1 band moves toward the X-point inside the FBZ. Far from X, its shape resembles an ellipsoid centered on the $0.85k_{\Gamma X}$ X-valley minimum. When approaching X, on the other hand, the shape diverges completely from the parabolic approximation and the contours (perpendicular to line ΓX) become highly warped, with extensions along line XU ($\langle 110 \rangle$ directions). In the X plane, these extensions meet at almost right angles on the XW segments, as indicated by the arrows: at these points, Δ_1 and $\Delta_{2'}$ bands are degenerate. The surface corresponding to $\Delta_{2'}$ has been plotted toward the outside of the FBZ (e.g., in the adjacent FBZ) for clarity. It extends in some respect the former one: in the X-U-W plane, it indeed prolongs the arcs of ellipse of Δ_1 so that its cusps appear as the intersection of two ellipses. As soon as one leaves the X-U-W plane, the degeneracy is lifted, and the anticrossing structure appears. It should be noted that this second convex shaped surface is (also) inside the former one. Its lateral extent decreases very rapidly and vanishes at a small distance from point X.

The degeneracy points indicated by the arrows should be, as suggested above, very sensitive to the strain and should induce enhancement of the higher-order terms in the deformation-potential $\mathbf{k}\cdot\mathbf{p}$ expansion. Furthermore, it may be easily verified that the strong warping shown here persists even at energies below that of the X point, and exists as soon as the surface approaches this point.

All these elements suggest that the effect of strain on band structure strongly affects the electrons, which become sensitive to these regions of reciprocal space in our accumulation layers.

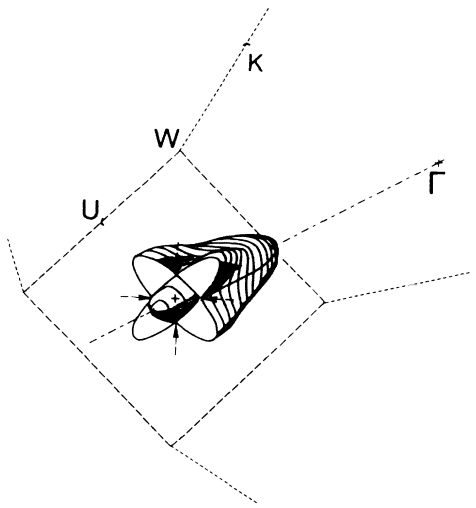

FIG. 6. Constant-energy surface of the silicon conduction band near the X point; the energy is 170 meV above that of the X point; contours perpendicular to line ΓX are plotted. The $\Delta_{2'}$ band (small protruding "nose") is plotted in the adjacent Brillouin zone for clarity. The four arrows denote the degenerate points whose sensitivity to strain may be enhanced.

V. CONCLUSION

We have analyzed the mobility data of our experiments on very-high-density accumulation layers at the n-type-Si/electrolyte interface, using PEO-based indifferent polymer electrolytes and a methanol-based electrolyte. The dependence of the mobility upon temperature T and density N_s is of the form $N_s^{-\alpha}T^{-\beta}$ ($0.3<\alpha<0.7$, $1.0<\beta<1.5$) at the very high concentrations studied here (up to $4.5\times10^{13}e^-/\mathrm{cm}^2$) whereas the observed order of magnitude of the mobility is very low (~ 100 cm^2/V s). Its temperature dependence in particular has prompted us to study acoustic-phonon and intervalley-phonon scattering of electrons in a two-dimensional layer at the silicon (111) surface. A more correct treatment has been obtained for intervalley phonons. It shows why the three-dimensional intervalley phonons are still relevant but also how the 2D matrix element has to be derived, including, if necessary, terms depending on the electron wave vector rather than the phonon wave vector only. With this proper formulation, and taking into account degeneracy effects, we find, however, that the mobility values, computed from acoustic-phonon and intervalley-phonon scattering, overestimate experimental data by a factor of 5–10. Attempts to explain similar but smaller discrepancies observed in the case of MOSFET-type Si electron layers were based mostly on possible interface-phonon peculiarities such as the "surfons" studied by Ezawa *et al.* with limited results. The increased discrepancy observed in our accumulation layers at very high densities has prompted us to take into account peculiarities of these highly concentrated electron systems. We propose that the increased band occupancy caused by the high densities makes the electrons sensitive to higher-order terms in the deformation-potential $\mathbf{k}\cdot\mathbf{p}$ expansion, thus leading to an overall increase of the acoustic-phonon-induced scattering. We introduce a tractable theoretical approach, using a "linear-in-k" deformation potential as the first term of this expansion; only one additional constant, $D_k=10^{-8}$ eV m, is used. We suggest that the peculiarities of the band structure of silicon may account for the strength of the higher-order terms and thus be responsible for the low order of magnitude of the observed mobility: degeneracies in the conduction band lie only at about 100 meV above the bottom of the conduction band. Finally, our simple theoretical approach, aimed at describing simply these higher-order terms, yields a good explanation for our mobility data but also for those relative to the common electron layers of high-density room-temperature MOSFET's.

ACKNOWLEDGMENTS

We wish to thank Professor K. Kunc for his help with band-structure calculations and Dr. B. Vinter for several useful discussions. Laboratoire de Physique de la Matière Condensée is Unité Associée D-1254 du Centre National de la Recherche Scientifique, France.

APPENDIX A: ANALYTICAL EVALUATION OF THE "LINEAR-IN-k" MECHANISM

We start from Eq. (34), which defines the equivalent $I_k(q_z)$ of $I(q_z)$ appearing in the squared modulus of the two-dimensional matrix element:

$$I_k(q_z)=\int_{-\infty}^{+\infty}\frac{dk_z}{2\pi}\Phi^*(k_z+q_z)\Phi(k_z)R(\mathbf{k},\mathbf{k}+\mathbf{q}) . \quad \text{(A1)}$$

For the Fang-Howard approximated fundamental wave function Eq. (9), we have

$$\Phi(k_z)=2\left[\frac{2}{b}\right]^{1/2}\left[1+2\frac{ik_z}{b}\right]^{-2} , \quad \text{(A2)}$$

$$I_k(q_z)=\int_{-\infty}^{+\infty}\frac{dk_z}{2\pi}\frac{8}{b}\left[1+2\frac{ik_z}{b}\right]^{-2}\times\left[1-2\frac{i(k_z+q_z)}{b}\right]^{-2}R(\mathbf{k},\mathbf{k}+\mathbf{q}) . \quad \text{(A3)}$$

We introduce the reduced variable

$$u=(2k_z+q_z)/b \quad \text{and} \quad u_z=q_z/b , \quad \text{(A4)}$$

so that the integral now reads

$$I_k(q_z)=\int_{-\infty}^{+\infty}du\ \frac{2}{\pi}[(1-iu_z)^2+u^2]^{-2}R(\mathbf{k},\mathbf{k}+\mathbf{q}) . \quad \text{(A5)}$$

In our case, the R function is

$$\begin{aligned}R(\mathbf{k},\mathbf{k}')&=[k^2+(k')^2]^{1/2}\\&=[k_\parallel^2+(k_\parallel')^2+k_z^2+(k')_z^2]^{1/2}\\&=\frac{b\sqrt{2}}{2}(u_\parallel^2+u_z^2+u^2)^{1/2} ,\end{aligned} \quad \text{(A6)}$$

where we use $\mathbf{k}'=\mathbf{k}+\mathbf{q}$ to get the right-hand term and we have also introduced

$$u_\parallel^2=2[k_\parallel^2+(k_\parallel')^2]/b^2 . \quad \text{(A7)}$$

This variable avoids making any difference between the elastic and inelastic cases. Taking finally

$$\alpha^2=u_\parallel^2+u_z^2,\quad \beta=1-iu_z , \quad \text{(A8)}$$

we obtain

$$I_k(q_z)=\frac{b\sqrt{2}}{\pi}\frac{1}{\beta^4}\int_{-\infty}^{+\infty}du(\alpha^2+u^2)^{1/2}[1+(u/\beta)^2]^{-2} . \quad \text{(A9)}$$

This intermediate form will be of some interest. To calculate it in the present we use the complex variable v defined by $\tan v=u/\beta$; one can check that v does not meet the poles of the tan function. The integral reduces to

$$\begin{aligned}I_k(q_z)&=\frac{b\sqrt{2}}{\pi\beta^3}\int_{-\pi/2}^{\pi/2}dv\frac{(\alpha^2+\beta^2\tan^2 v)^{1/2}}{1+\tan^2 v}\\&=\frac{b\sqrt{2}}{\pi\beta^3}\int_{-\pi/2}^{\pi/2}dv(\alpha^2\cos^2 v+\beta^2\sin^2 v)^{1/2}\cos v ,\end{aligned} \quad \text{(A10)}$$

or similarly, with $w=\sin v$, w running from -1 to 1,

$$I_k(q_z)=\frac{b\sqrt{2}}{\pi\beta^3}\int_{-1}^{1}dw[\alpha^2+(\beta^2-\alpha^2)w^2]^{1/2} . \quad \text{(A11)}$$

Finally,

$$I_k(q_z)=\frac{b\sqrt{2}}{\pi\beta^3}\left[\beta+\frac{\alpha^2}{(\beta^2-\alpha^2)^{1/2}}\mathcal{L}\left[\frac{\beta^2-\alpha^2}{\alpha^2}\right]^{1/2}\right] , \quad \text{(A12)}$$

where the Argsinh function is defined by $\mathcal{L}(x)=\ln[x+(x^2+1)^{1/2}]$, ln being the complex logarithm.

The squared modulus $|I_k(q_z)|^2$ contains the factor $|1/\beta^3|^2$ which is indeed the usual expression $|I(q_z)|^2$. To carry out further computations more easily, I_k may be conveniently approximated writing first from Eq. (A9):

$$|I_k(q_z)|^2=\frac{2b^2}{\pi^2}\int_{-\infty}^{+\infty}du'\int_{-\infty}^{+\infty}du\frac{(\alpha^2+u^2)^{1/2}}{(\beta^2+u^2)^2}\frac{[\alpha^2+(u')^2]^{1/2}}{(\beta^{*2}+u^2)^2} \quad \text{(A13)}$$

and approximating the numerator to keep only terms symmetrical in u,u':

$$(\alpha^2+u^2)^{1/2}[\alpha^2+(u')^2]^{1/2}\approx\alpha^2+|uu'| , \quad \text{(A14)}$$

so that one can write

$$|I_k(q_z)|^2\approx\frac{2b^2}{\pi^2}\alpha^2\left|\int_{-\infty}^{+\infty}du\frac{1}{(\beta^2+u^2)^2}\right|^2+\frac{2b^2}{\pi^2}\left|\int_{-\infty}^{+\infty}du\frac{|u|}{(\beta^2+u^2)^2}\right|^2 , \quad \text{(A15)}$$

and one uses again $\tan v=u/\beta$ to carry out the summations. We get the "bilinear approximation" in reduced or standard variables, focusing on the elastic case for this latter expression:

$$|I_k(q_z)|^2\approx(1+u_z^2)^{-3}\left[\frac{2b^2}{\pi^2}\right]\left[1+\frac{\pi^2}{4}u_\parallel^2+\left[1+\frac{\pi^2}{4}\right]u_z^2\right] , \quad \text{(A16)}$$

$$|I_k(q_z)|^2\approx|I(q_z)|^2\left[\frac{2}{\pi^2}\right]\left[b^2+\pi^2k_\parallel^2+\left[1+\frac{\pi^2}{4}\right]q_z^2\right] .$$

The bilinear expression between the braces of the first expression above is shown in Fig. 7 (dashed line) as a function of the reduced quantities $u_\parallel^2=4k_\parallel^2/b^2$ and $u_z^2=q_z^2/b^2$; it is compared to the corresponding analytical result $(|I_k(q_z)|^2/|I(q_z)|^2)\times\pi^2/2b^2$ (solid line). The

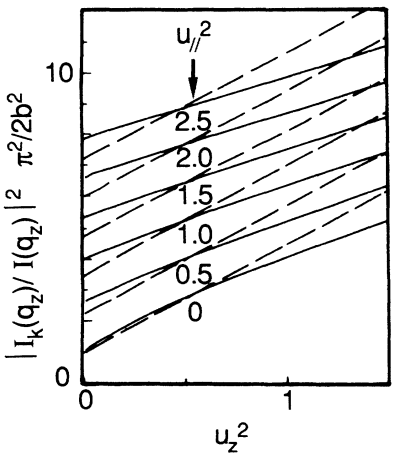

FIG. 7. Bilinear approximation (dashed lines) and exact computation (solid lines) of the reduced ratio $|I_k(q_z)/I(q_z)|^2\times\pi^2/2b^2$ as a function of the reduced parameter $u_{\parallel}^2=4k_{\parallel}^2/b^2$.

agreement is good in the region of interest $0<q_z/b<1$. This approximation avoids the numerical integration of $|I_k(q_z)|^2$, the last step to obtain the 2D matrix element. This is further justified in Fig. 8 by comparing the integration of the bilinear approximation (dashed line) to the result of the numerical integration, which is almost an affine function of $k_{\parallel}^2$ in this region. The equation of such an affine approximation reads

$$J_k=\int_{-\infty}^{+\infty}\frac{dq_z}{2\pi}|I_k(q_z)|^2\approx b(A_0b^2+A_1k_{\parallel}^2)\ . \qquad \text{(A17)}$$

In order to fit better the exact result at $k=0$, we have chosen the A_0 and A_1 coefficients slightly different from those given by the bilinear approximation: $A_0=0.0784$ and $A_1=0.426$, instead of $A_0=1/(2\pi^2)+\frac{1}{32}\approx0.0819$ and $A_1=\frac{3}{8}=0.375$ from the bilinear approximation.

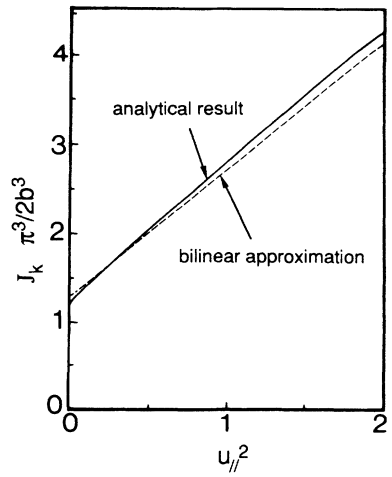

FIG. 8. Plot of the factor $J_k=\int|I_k(q_z)|^2\,dq_z/2\pi$ entering the scattering rate from the bilinear approximation [Eq. (A17), dashed line] and from the exact computation (solid line).

APPENDIX B: FIRST-ORDER OPTICAL-PHONON SCATTERING IN TWO DIMENSIONS

We start from the inelastic version of Eq. (B3), substituting back $2k_{\parallel}^2$ by $k_{\parallel}^2+(k'_{\parallel})^2$:

$$J_k=A_0b^2+\frac{A_1bm_D^*E}{\hbar^2}+\frac{A_1}{2}b(k'_{\parallel})^2 \qquad \text{(B1)}$$

We now have to compute the scattering rate from Eq. (15), using the Fermi golden rule to relate $P(\mathbf{k},\mathbf{k}')$ to the 2D matrix element (absorption or emission):

$$\frac{1}{\tilde\tau_{\pm}^{2D,g}(E)}=\left[\frac{D_1^2}{2\pi\rho\omega_q}\right]\int d^2k'_{\parallel}\,J_k(n_q+\tfrac12\pm\tfrac12)\times\frac{1-f_0(E')}{1-f_0(E)}\delta(E'-E\pm\hbar\omega_q)\ . \qquad \text{(B2)}$$

The tilde is used to distinguish Eq. (B2) from Eq. (17) of Sec. III. The term in $(k'_{\parallel})^2$ of Eq. (B1) is integrated using:

$$\int d^2k'_{\parallel}\,(k'_{\parallel})^2\delta(E'-E\pm\hbar\omega_q)=\frac{4\pi(m_D^*)^2}{\hbar^4}(E\pm\hbar\omega_q)\Theta(E\pm\hbar\omega_q) \qquad \text{(B3)}$$

The terms containing A_1E are then gathered to yield Eq. (37), the Heaviside function being omitted:

$$\frac{1}{\tilde\tau_{\pm}^{2D,g}(E)}=\frac{m_D^*b}{2\rho\hbar^2\omega_q}D_1^2\left[A_0b^2+\frac{A_1m_D^*}{\hbar^2}(2E\pm\hbar\omega_q)\right]\times(n_q+\tfrac12\pm\tfrac12)\frac{1-f_0(E\pm\hbar\omega_q)}{1-f_0(E)}\ . \qquad \text{(B4)}$$

Let us compare to Eq. (17); using $J=3b/16$, we find the ratio:

$$\frac{[\tilde\tau_{\pm}^{2D,g}(E)]^{-1}}{[\tau_{\pm}^{2D,g}(E)]^{-1}}=\tfrac83\left[A_0\frac{\hbar^2b^2}{m_D^*(2E\pm\hbar\omega_q)}+A_1\right]\ . \qquad \text{(B5)}$$

Using the bilinear approximation $A_1=\frac38$, $A_0=(1/2\pi^2)+\frac{1}{32}$, we have

$$\frac{[\tilde\tau_{\pm}^{2D,g}(E)]^{-1}}{[\tau_{\pm}^{2D,g}(E)]^{-1}}=1+\left[\frac{4}{3\pi^2}+\tfrac{1}{12}\right]\frac{\hbar^2b^2/m_D^*}{(2E\pm\hbar\omega_q)}\approx1+0.22\frac{2E(k=b)}{2E\pm\hbar\omega_q}\ . \qquad \text{(B6)}$$

This ratio is therefore comparable to 1 for most values of the energy. When the denominator vanishes, both scattering rates vanish as well. The case of a predominant first-order mechanism seems necessary to check the validity of Eq. (B4) compared to the Ferry-like expression Eq. (17). In our computations, the effect of this mechanism is so small that a change is barely seen on any of the mobility curves. We have therefore used Eq. (17) in our mobility computations for simplicity and ease of comparison.

APPENDIX C: CROSSED INTERFERENCE TERM

If we want to take into account the hypothesis that both the usual deformation potential and our "linear-in-k" mechanisms are in phase, we must calculate the squared modulus of an expression containing $[DI(q_z)]$ for the former and $[D_k I_k(q_z)]$ for the latter. The squared modulus yields an interference term:

$$|DI(q_z)+D_k I_k(q_z)|^2=D^2|I(q_z)|^2+D_k^2|I_k(q_z)|^2 +2DD_k\,\mathrm{Re}[I(q_z)I_k(q_z)] . \quad \text{(C1)}$$

This term may be evaluated from Eq. (A12) and integrated numerically. Plotting this integral as a function of $u_{\parallel}^2$, one readily sees that an excellent approximation is given by

$$\int_{-\infty}^{+\infty}\frac{dq_z}{2\pi}2\,\mathrm{Re}[I(q_z)I_k^{*}(q_z)]=b(B_0b^2+B_1k_{\parallel}^2)^{1/2} , \quad \text{(C2)}$$

with $B_0\approx 0.0496$ and $B_1\approx 0.33$, which recalls us the expression of the integral of $|I_k(q_z)|^2$ in the text.

In the numerical evaluation of the scattering rate, we assume that DD_k is positive, i.e., that both effects interfere constructively.

[1] T. Ando, A. B. Fowler, and F. Stern, Rev. Mod. Phys. **54**, 499 (1982).

[2] S. M. Sze, *Physics of Semiconductors Devices*, 2nd ed. (Wiley Interscience, New York, 1981).

[3] T. Sato, Y. Takeishi, H. Hara, and Y. Okamoto, Phys. Rev. B **4**, 1950 (1971).

[4] H. Ezawa, S. Kawaji, and K. Nakamura, Jpn. J. Appl. Phys. **13**, 126 (1974).

[5] P. Stallhofer, J. P. Kotthaus, and G. Abstreiter, Solid State Commun. **32**, 655 (1979).

[6] B. Vinter, Solid State Commun. **32**, 651 (1979).

[7] A. Tardella and J.-N. Chazalviel, Phys. Rev. B **32**, 2439 (1985).

[8] M. Wolovelsky, J. Levy, Y. Goldstein, A. Many, S. Z. Weisz, and O. Resto, Surf. Sci. **171**, 442 (1986).

[9] H. Benisty and J.-N. Chazalviel, Appl. Phys. Lett. **51**, 1121 (1987).

[10] H. Gerischer, in *Physical Chemistry; An Advanced Treatise*, Vol. IXA of *Electrochemistry*, edited by H. Eyring (Academic, New York, 1970), pp. 463–542.

[11] C. A. Barlow, Jr., in *Physical Chemistry; An Advance Treatise*, Vol. IXA of *Electrochemistry*, edited by H. Eyring (Academic, New York, 1970), pp. 181–189.

[12] S. R. Morrison, *Electrochemistry at Semiconductor and Oxidized Metal Electrodes* (Plenum, New York, 1980).

[13] D. T. Sawyer and J. L. Robert, Jr., *Experimental Electrochemistry for Chemists* (Wiley, New York, 1974).

[14] H. Benisty and J.-N. Chazalviel, J. Electrochem. Soc. **137**, 1209 (1990).

[15] W. A. Harrison, Phys. Rev. **104**, 1281 (1956).

[16] J.-N. Chazalviel, J. Electroanal. Chem. **233**, 37 (1987).

[17] D. Roychoudhury and P. K. Basu, Phys. Rev. B **22**, 6325 (1980).

[18] S. Kawaji, J. Phys. Soc. Jpn. **27**, 906 (1969).

[19] D. K. Ferry, Phys. Rev. B **14**, 5364 (1976).

[20] D. Long, Phys. Rev. **120**, 2024 (1960).

[21] D. K. Ferry, Surf. Sci. **57**, 218 (1976).

[22] K. Hirakawa and H. Sakaki, Phys. Rev. B **33**, 8291 (1986).

[23] F. Stern, Phys. Rev. Lett. **44**, 1469 (1980).

[24] F. F. Fang and W. E. Howard, Phys. Rev. Lett. **16**, 797 (1966).

[25] B. R. Nag, *Theory of Electrical Transport in Semiconductors* (Pergamon, Oxford, 1972).

[26] Electric-field induced ionicity has been studied in diamond by E. Anastassakis and E. Burstein, Phys. Rev. B **2**, 1952 (1970). It involves the constant a appearing in the Raman tensor. From several sources [H. Wendel, Solid State Commun. **31**, 423 (1979); M. Grimsdich and M. Cardona, in *Physics of Semiconductors 1978*, Inst. Phys. Conf. Ser. No. 43, edited by B. Wilson (IOP, London, 1978), p. 639; J. P. Russel, Appl. Phys. Lett. **6**, 223 (1965)], we take $a\approx 25$ Å^2 (Gauss system units); at the high fields attainable at the accumulated Si/electrolyte interface, say 8×10^8 V/m, the ionicity reaches as much as $0.14|e|$. However, the resulting scattering yields mobility values in the 500–1000 cm^2/Vs range, still largely in excess of experimental values. As for the behavior as a function of N_s, this ionicity is proportional to the electric field and thus to the areal charge eN_s, so that any related matrix element will scale as N_s and its square like N_s^2, which is actually too steep to fit our results.

[27] C. Herring and E. Vogt, Phys. Rev. **101**, 944 (1956).

[28] M. H. Jørgensen, Phys. Rev. B **18**, 5657 (1978).

[29] M. L. Cohen and T. K. Bergstresser, Phys. Rev. **141**, 789 (1966).

[30] J. R. Chelikowsky and M. L. Cohen, Phys. Rev. B **14**, 556 (1976).

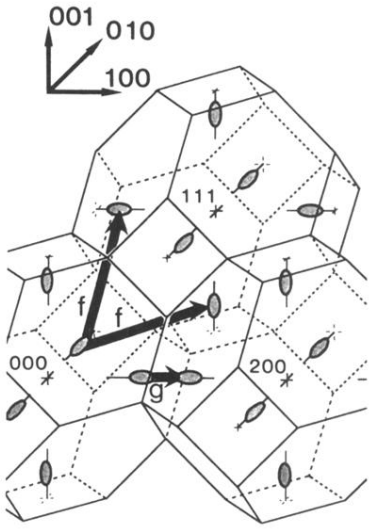

FIG. 2. Intervalley *umklapp* f and g phonons in the silicon reciprocal lattice; three adjacent first Brillouin zones are used. The valleys are represented by constant-energy ellipsoids.